We are IntechOpen, the world's leading publisher of Open Access books Built by scientists, for scientists

6,900
Open access books available

185,000
International authors and editors

200M
Downloads

Our authors are among the

154
Countries delivered to

TOP 1%
most cited scientists

12.2%
Contributors from top 500 universities



WEB OF SCIENCE™

Selection of our books indexed in the Book Citation Index in Web of Science™ Core Collection (BKCI)

Interested in publishing with us?
Contact book.department@intechopen.com

Numbers displayed above are based on latest data collected.
For more information visit www.intechopen.com



Chapter

Optical Fibers Profiling Using Interferometric and Digital Holographic Methods

Hamdy Wahba, Wael Ramadan and Ahmed El-Tawargy

Abstract

Optical fibers are extensively used in modern technology such as sensing, short-distance and long-distance telecommunications. This motivated many researchers to present different methods in order to characterize optical fibers and determine their refractive index profiles. In addition, variation of refractive index profiles of optical fibers suffering mechanical stresses or other external effects reflects good information about the internal structure of these fibers and how they are responding to these external effects. Optical interferometry and digital holography methods are accurate and effective tools used to achieve this task. In this chapter, we illustrate the application of different types of optical interference on conventional, polarizing maintaining and thick optical fibers. Also, we illustrate some mathematical interpretations (and recently automatic analyzing of interference patterns) that have been used to reconstruct the accurate refractive index profiles of optical fibers. Some experimental interferograms and refractive index profiles are demonstrated as well.

Keywords: optical fiber, optical interferometry, refractive index profile, interferogram analyses, digital holography

1. Introduction

1.1 Optical fibers

An optical fiber is an extended cylindrical optical waveguide. In its simplest form, it consists of a core having a certain refractive index n_c and is surrounded by a clad (sometimes called skin) of refractive index n_{cl} (or n_s). An optical fiber is used to guide light through its core, from one end to another, based on the principle of total internal reflection which mandates that n_c must be always higher than n_{cl}. Basically, optical fibers are made of highly pure silica glass doped with some impurities in order to increase n_c or decrease n_{cl} [1–3]. Recently, polymeric optical fibers got more attention as alternatives of some glass based optical fibers [1, 4].

Optical fibers are involved in many technological applications such as telecommunications, sensing [4, 5]; fiber lasers and fiber amplifiers [6]; fiber gratings which can act as mirrors [7, 8]; mode converters [9]; modulators; and couplers and switches [10, 11]. Optical fibers are considered ideal optical transmission media since communication cables hundreds of kilometers in length can be obtained with

IntechOpen

low absorption and low loss due to the purity and cross-sectional uniformity of the manufactured optical fibers. Moreover, accurate tuning of the refractive indices of both core and clad guarantee extremely low scattering loss at the interfaces [1].

1.2 Types of optical fibers

The commonly known optical fibers are step index and graded index (GR-IN) optical fibers. The former means that the core's refractive index is homogeneous while it suffers an abrupt change at the boundary with the clad. For a GR-IN optical fiber, the core does not have a constant value of refractive index but it rather has a radial distribution of refractive index. These two types of optical fibers can be classified into either single-mode or multi-mode optical fibers. Single-mode optical fiber only sustains one mode of propagation while the multi-mode optical fiber can sustain up to hundreds of propagation modes [1, 3]. The number of the propagation modes is related to the numerical aperture of the fiber, which, in turn, depends on the refractive indices of both core and clad.

1.3 Characterization of optical fibers

Accurate characterization of optical fibers is required in order to know about their functions and performances. There are many methods of optical fibers characterization such as optical microscopy, electron microscopy, X-ray spectrometry, infrared spectroscopy, light diffraction, light scattering, optical interferometry, and digital holography [1, 3, 12–29]. Optical interferometry is an effective accurate tool for studying and characterizing optical fibers. It depends on the determination of the phase difference between a ray of light transmitting the fiber's cross-section and a reference ray reaching the interference plane directly without crossing the fiber. This phase shift can be transformed into a refractive index map representing the radial distribution of the refractive index across the fiber or, in other words, the refractive index profile (RIP). Interferometry can detect tiny changes in refractive index if an external effect is applied on the fiber. The change of refractive index can be in situ detected if the interferometer is developed to achieve this task. Interference patterns can be digitally processed and analyzed in order to increase the accuracy of the obtained results [1, 17, 22, 26, 27, 30–35].

Interference techniques can be classified into either two-beam interferometers such as Michelson, Mach-Zehnder, Pluta polarizing microscope, Lioyd's mirror, etc., or multiple-beam interferometers such as Fabry-Pérot and Fizeau interferometers [1, 3, 25, 36–39]. A two-beam interferometer produces a pattern of alternate bright and dark fringes of equal thicknesses when two beams, usually, of equal intensities I_o suffering a relative phase difference δ are superposed. The resultant intensity distribution I of the interference pattern is given as:

$$I = I_o \cos^2\left(\frac{\delta}{2}\right) \tag{1}$$

Multiple-beam interference takes place when light rays fall on two parallel optical plates enclosing a small distance between each other while their inner surfaces are highly reflecting and partially transparent. The intensities of both reflected, $I^{(r)}$, and transmitted, $I^{(t)}$, light distributions that are redistributed due to the multiple-beam interference are given as [40]

$$I^{(r)} = \frac{(2 - 2\cos\delta)R}{1 + R^2 - 2R\ \cos\ \delta} I^{(i)} \tag{2}$$

$$I^{(t)} = \frac{T^2}{1 + R^2 - 2R\ \cos\ \delta} I^{(i)} \tag{3}$$

where, $I^{(i)}$ is the intensity of the incident light, T and R are the products of the transmission and reflection coefficients of the two surfaces, respectively, while δ is the phase difference between any two consecutive interfered rays.

On the other hand, holography was firstly presented by Gabor in 1947 as a lensless process for image formation by reconstruction of wave-fronts [41–43]. It offers 3D characterization such as the depth of field from recording and reconstructing the whole optical wave field, intensity, and phase [41, 42]. Holographic interferometry is a non-destructive, contactless tool that can be used for measuring shapes, deformations and refractive index distributions [44, 45]. The modern digital holography was introduced in 1994 [46–48]. Moreover, the phase shifting interferometric (PSI) technique was introduced by Hariharan et al. as an accurate method for measuring interference fringes in the real time [49]. Recently, digital holographic phase shifting interferometry (DHPSI) was used to investigate some optical parameters of fibrous materials [17, 18, 21, 26–29].

1.4 Digital holographic phase shifting interferometry (DHPSI)

In DHPSI, frequently a set of four [20] or five [23, 33] phase shifted holograms with known mutual phase shifts starting with 0^0 and having 90^0 separations have to be recorded [21]. These recorded holograms can be represented by:

$$I_n = a(\zeta, \eta) + b(\zeta, \eta)\cos\left(\varphi(\zeta, \eta) + \varphi_{Rn}\right), n = 1, 2, 3, \ldots \tag{4}$$

where $a(\zeta, \eta)$ and $b(\zeta, \eta)$ are the additive and the multiplicative distortions and φ_{Rn} is the phase shift of the reference wave. In case of four and five phase shifted holograms, the complex wavefield [37] in the hologram plane can be calculated using Eqs. (5) and (6), respectively.

$$h(\zeta, \eta) = [I_1(\zeta, \eta) - I_3(\zeta, \eta)] + i[I_4(\zeta, \eta) - I_2(\zeta, \eta)] \tag{5}$$

or,

$$h(\zeta, \eta) = [4I_1(\zeta, \eta) - I_2(\zeta, \eta) - 6I_3(\zeta, \eta) - I_4(\zeta, \eta) + 4I_5(\zeta, \eta)] + i[7(I_4(\zeta, \eta) - I_2(\zeta, \eta))] \tag{6}$$

In digital holography, the recorded wavefield is reconstructed, based on Fresnel diffraction integral, by multiplying the stored hologram by the complex conjugate of the reference wave $r^*(\zeta, \eta)$ to calculate the diffraction field $b'(x', y')$ in the image plane, see **Figure 1**. This can be calculated using the finite discrete form of the Fresnel approximation to the diffraction integral as:

$$b'(n\Delta x', m\Delta y') = A\sum_{j=0}^{N-1}\sum_{l=0}^{M-1} h(j\Delta\zeta, l\Delta\eta) r^*(j\Delta\zeta, l\Delta\eta) \times exp\left\{\frac{i\pi}{d'\lambda}\left(j^2\Delta\zeta^2 + l^2\Delta\eta^2\right)\right\} exp\left\{2i\pi\left(\frac{jn}{N} + \frac{lm}{M}\right)\right\} \tag{7}$$

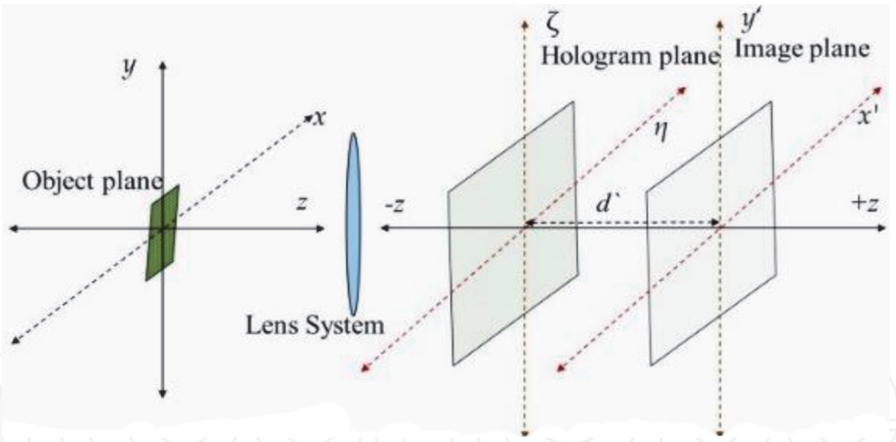


Figure 1.
Geometry of digital holographic axes and the planes systems.

The parameters used in this formula depend on the used CCD array of $N \times M$ pixels and the pixel pitches $\Delta\zeta$ and $\Delta\eta$. The distance between the hologram and the image plane is denoted by d'. The pixel spacings in the reconstructed field of image are:

$$\Delta x' = \frac{d'\lambda}{N\Delta\zeta} \; and \; \Delta y' = \frac{d'\lambda}{M\Delta\eta} \tag{8}$$

The convolution of $h(\zeta, \eta)r^*(\zeta, \eta)$ can be used as alternative of Fresnel approximation [37]. The resulting pixel spacing for this convolution approach is

$$\Delta x' = \Delta\zeta \; and \; \Delta y' = \Delta\eta \tag{9}$$

In addition, the phase shifted holograms are used to overcome the problems of the d.c. term and twin image, in which the calculated complex wavefield is used instead of a real hologram in the convolution approach.

The intensity and phase distributions in the reconstruction plane are given by

$$I(x', y') = |b'(x', y')|^2 \tag{10}$$

$$\varphi(x', y') = arctan\left\{\frac{Im|b'(x', y')|}{Re\,|b'(x', y')|}\right\} \tag{11}$$

So, the optical phase differences due to phase objects can be extracted.

Mach-Zehnder interference-like system is used as a digital holographic setup as shown in **Figure 2** [20, 23, 29, 33]. The optical waveguide sample, such as optical fiber, is immersed in a liquid of refractive index n_L near or matching the cladding refractive index n_{clad} of the sample. The interference patterns are recorded using a charge-coupled device, that is, CCD camera.

In this chapter, we illustrate some featured work on interferometric characterization (sometimes, implying digital holographic interferometry) of different optical fibers done by our research group during the last three decades. In Section 2, interferometric characterization of conventional step-index and GR-IN optical fibers is presented. Section 3 illustrates characterization of the conventional optical fibers when they are suffering mechanical bending. In Section 4, interferometric characterization of a special type of optical fibers called polarization maintaining (PM) optical fibers is presented. In the last section, we elucidate thick optical

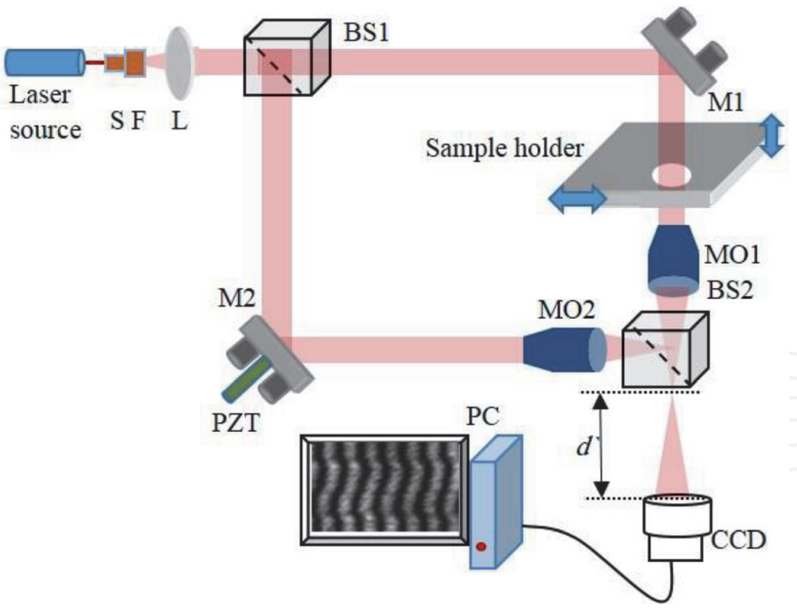


Figure 2.
Mach-Zehnder digital holographic interferometric set-up, S F: spatial filter, L: collimating lens, BS: beam splitter, M: mirror, and MO: microscopic objective.

fibers and their interferometric characterization with a special interferometric system, developed in our laboratory, called lens-fiber interferometry (LFI).

2. Conventional optical fibers

2.1 Step-index optical fiber

In 1994, Hamza et al. derived a mathematical expression to calculate the RIP of an optical fiber by considering the refraction of optical rays at the liquid-clad and clad-core interfaces, see **Figure 3** [12]. It was the first time to consider the refraction of the transmitted rays to reconstruct the RIP of a fiber. The derived expressions for calculating the RIP in case of two-beam and multiple-beam interferences, based on **Figure 3**, are given by Eqs. (12) and (13), respectively.

$$\frac{Z(x)\lambda}{h} = 2n_s\left\{\sqrt{\left[R^2-\left(\frac{n_L d}{n_s}\right)^2\right]}-\sqrt{\left[(R-e)^2-\left(\frac{n_L d}{n_s}\right)^2\right]}\right\} + 2n_c\sqrt{\left[(R-e)^2-\left(\frac{n_L d}{n_c}\right)^2\right]}-n_L\left[\sqrt{\left(R^2-d^2\right)}+\sqrt{\left(R^2-x^2\right)}\right]\ 0\le d<R \tag{12}$$

$$\frac{Z(x)\lambda}{2h} = 2n_s\left\{\sqrt{\left[R^2-\left(\frac{n_L d}{n_s}\right)^2\right]}-\sqrt{\left[(R-e)^2-\left(\frac{n_L d}{n_s}\right)^2\right]}\right\} + 2n_c\sqrt{\left[(R-e)^2-\left(\frac{n_L d}{n_c}\right)^2\right]}-n_L\left[\sqrt{\left(R^2-d^2\right)}+\sqrt{\left(R^2-x^2\right)}\right]\ 0\le d<R \tag{13}$$

where, R is the fiber's radius and e is the skin's thickness. n_L, n_s, and n_c are the refractive indices of the immersion liquid, skin, and core, respectively. λ is the wavelength of the used illuminating source. L_s and L_c are the geometrical path lengths inside the skin and the core, respectively. Z is the fringe shift due to the presence of the fiber while h is the interfringe spacing and d is the distance measured from the center of the fiber to the position of the incident ray.

In that work, they used Fizeau interferometer to determine the refractive index profile of FOS Ge-doped step-index multi-mode optical fiber with a core radius 19.5 μm. The fiber was immersed in a liquid of refractive index n_L = 1.4665, which was a little bit greater than n_s while the wavelength of the used illuminating source was λ = 546.1 nm. The Fizeau interferogram of this fiber is shown in **Figure 4a**. The obtained RIP was compared with the profile calculated for the same fiber when the refraction of light through the fiber was neglected as was usually done by other authors before this work. There was a significant difference between the two profiles, see **Figure 4b**. Therefore, the refraction through the fiber was recommended to be considered for calculating RIPs particularly when the refractive index of the immersion liquid is not close to the fiber's refractive index.

In 2008, another mathematical model was derived in order to determine RIPs of fibers having regular and/or irregular cross-sections [38]. This method was based

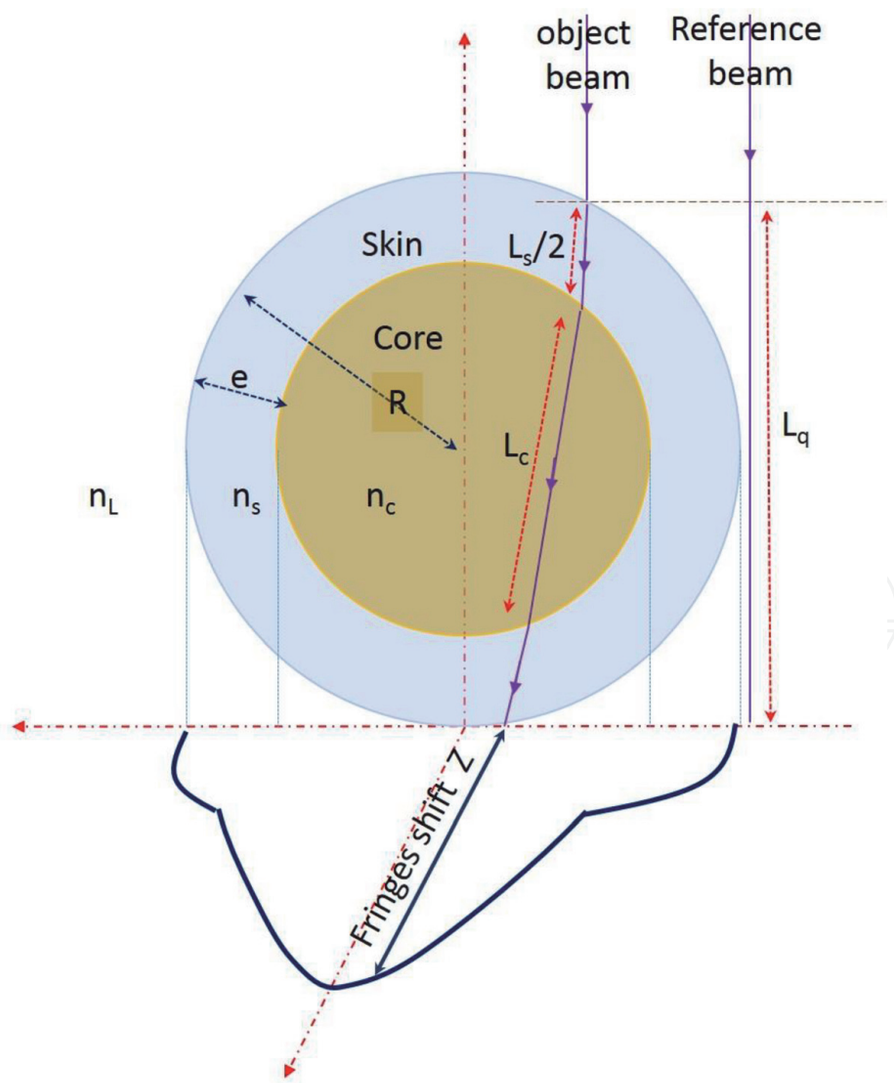


Figure 3.
An incident ray (object ray) is refracted due to a clad-core fiber causing a fringe shift Z when interferes with a reference ray.

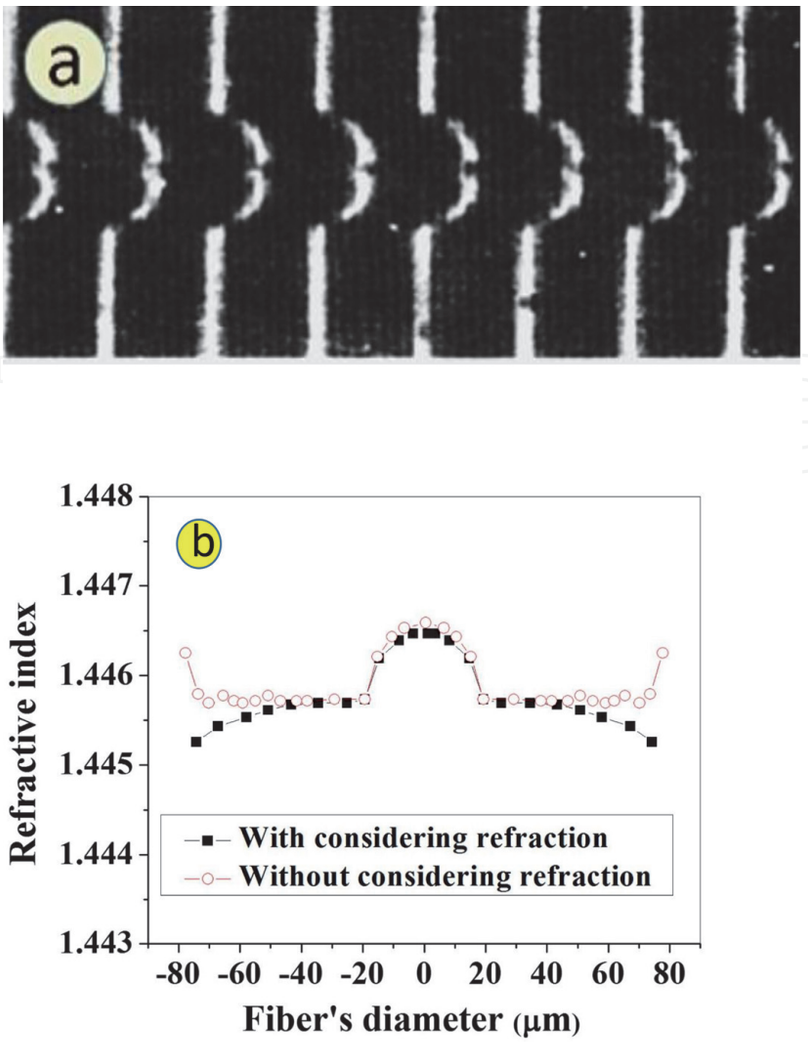


Figure 4.
(a) An interference pattern of Fizeau fringes, in transmission, for a FOS step-index optical fiber. (b) RIPs of this fiber in case of considering and neglecting the retraction of the crossing rays inside the fiber.

on immersing the investigated fiber in two liquids with different, but so closed, refractive indices. They applied this method on a single-mode optical fiber, having a small core of radius <5 μm while the fiber's radius was 60.6 μm, as shown by Fizeau interferograms in **Figure 5** when the fiber was immersed in two liquids with refractive indices (a) 1.4589 and (b) 1.4574. The obtained RIP of this fiber is illustrated in **Figure 5c** showing that this fiber has n_c = 1.4630 and n_{cl} = 1.4596. This method was simple and accurate enough to detect such a small core of a step-index optical fiber.

2.2 Graded-index (GR-IN) optical fiber

A GR-IN optical fiber with a radial refractive index distribution was suggested to be divided into a finite number (M) of concentric layers where each layer has its own value of refractive index, see **Figure 6a**. The thickness (a) of each layer equals R/M, where R is the radius of the graded-index part. When the ray falls on the fiber at a distance d_Q apart from the fiber's center, the ray refracts through Q layers. The nearest layer to the fiber's center has a refractive index n_Q. The fiber's RIP can be calculated using Eq. (14) in case of two-beam interference and Eq. (15) in case of multiple-beam interference [13]. Another model was presented in order to get RIP of a GR-IN optical fiber by considering the real path of the optical ray due to the

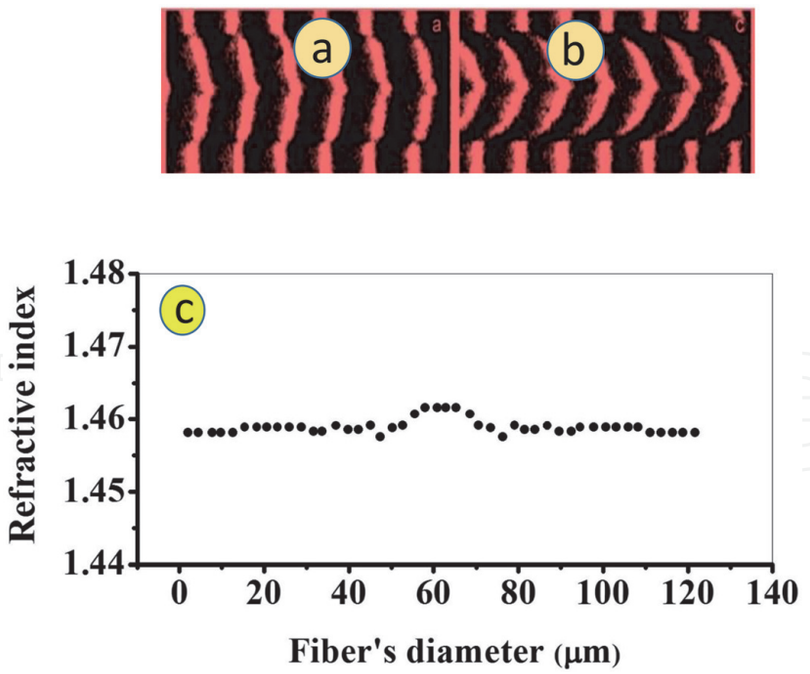


Figure 5.
Fizeau interferograms, in transmission, for a single-mode optical fiber when it was immersed in two liquids of refractive indices (a) 1.4589, (b) 1.4574. (c) RIP of the single-mode optical fiber having the interferograms shown in (a) and (b).

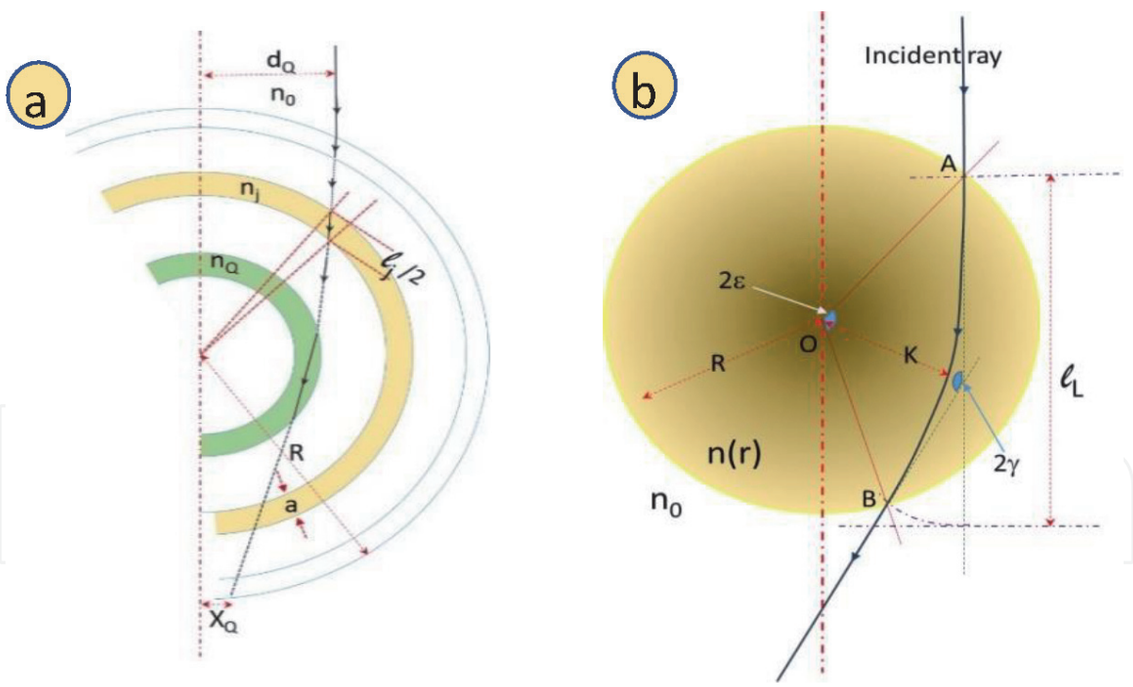


Figure 6.
(a) A schematic diagram shows the path of an optical ray crossing Q *layers in the core region. (b) A schematic diagram shows the path of an optical ray crossing a GR-IN core optical fiber.*

refraction in the core region as well as adding a correction for the ray passing through the immersion liquid [50], see **Figure 6b**. In this case, the fringe shift was obtained by assuming values for both the profile shape parameter (α) and the difference between refractive indices of core and clad (Δn). A prepared software was programmed to iterate and get the best values of α and Δn and comapre the calculated fringe shift with the experimentally obtained one.

$$\frac{\lambda Z_Q}{h} = \sum_{j=1}^{Q-1} 2n_j \left[\sqrt{(R-(j-1)a)^2 - \left(\frac{d_Q n_o}{n_j}\right)^2} - \sqrt{(R-ja)^2 - \left(\frac{d_Q n_o}{n_j}\right)^2} \right] + 2n_Q \sqrt{(R-(Q-1)a)^2 - \left(\frac{d_Q n_o}{n_Q}\right)^2} - n_o \left[\sqrt{R^2 - d_Q^2} + \sqrt{R^2 - x_Q^2} \right] \quad (14)$$

$$\frac{\lambda Z_Q}{2h} = \sum_{j=1}^{Q-1} 2n_j \left[\sqrt{(R-(j-1)a)^2 - \left(\frac{d_Q n_o}{n_j}\right)^2} - \sqrt{(R-ja)^2 - \left(\frac{d_Q n_o}{n_j}\right)^2} \right] + 2n_Q \sqrt{(R-(Q-1)a)^2 - \left(\frac{d_Q n_o}{n_Q}\right)^2} - n_o \left[\sqrt{R^2 - d_Q^2} + \sqrt{R^2 - x_Q^2} \right] \quad (15)$$

According to **Figure 6b**, the optical pathlengths of the ray crossing the core $Ol(K)$ and the ray passing only in the immersing liquid Ol_L are given by the following relations.

$$Ol(K) = 2\int_K^R \frac{n^2(r)r}{\sqrt{n^2(r)r^2 - n^2(K)K^2}} dr \quad (16)$$

$$Ol_L = 2n_o R \frac{\sin(\varepsilon)}{\sin(\gamma)} \quad (17)$$

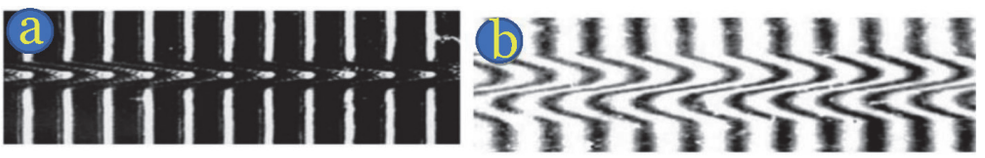


Figure 7.
(a) Pluta duplicated image of LDF GR-IN optical fiber and (b) Fizeau interferogram of the same sample. Reference [50] with permission.

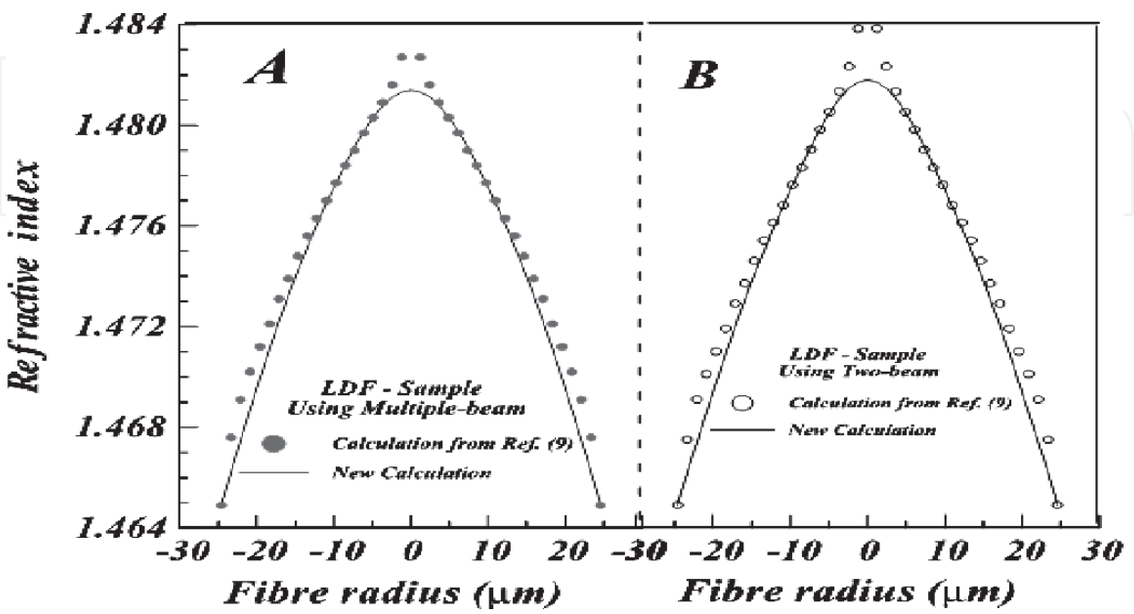


Figure 8.
A comparison between RIPs of LDF GR-IN optical fiber using the model in Ref. [27] (dots) and model in Ref. [28] (solid curve) in case of (a) multiple-beam Fizeau interference and (b) two-beam Pluta interference. Ref. [50] with permission.

where, R is the core's radius, k is the minimum distance between the fiber's center and the bent ray, ε is the half of the angle determined by the two radii that are enclosing the bent ray inside the graded-index region, and γ is the half of the angle between the incident and the emerged rays. **Figure 7** shows the interferograms of LDF GR-IN optical fiber when it was investigated by (a) Pluta and (b) Fizeau interferometers. **Figure 8** shows the RIPs calculated by these last models for the LDF optical fiber. The last model, presented in 2001 [50], provided more accurate values of the RIP of a GR-IN optical fiber compared with its previous presented model in Ref. [13].

However, the former requires knowing the function describing the index profile while the aim is to find the parameters of this function.

3. Bent conventional optical fibers

Optical fibers, which are isotropic materials, can suffer a birefringence under external mechanical bending effects [1, 22, 33, 51]. The induced birefringence can be used in sensing applications [52–54]. However, bending has an unfavorable effect on the optical fibers used in telecommunications where it, sometimes, causes a mode disturbance and consequently a signal attenuation [55, 56]. An approach to calculate the refractive index profile of a bent optical fiber was proposed where the fiber was divided into layers and slabs simultaneously [22]. The refraction of the optical rays at the liquid-clad and clad-core interfaces was considered. Unfortunately, this approach did not consider the change of refractive index inside each slab. Also, the expected change of refractive index due to the release of stresses near the fiber's free surface has not been considered. However, this approach succeeded to present good information about the variation of mode propagation due to bending.

3.1 Step-index bent conventional optical fiber

In 2014, Ramadan et al. calculated the refractive index and the induced birefringence profiles of bent step-index optical fibers using digital holographic Mach-Zehnder interferometer [33]. In that work, they considered two different processes controlling the variations of the refractive index of the bent fiber: (1) the linear refractive index variation due to the applied stress along the bent radius and (2) the release of this stress on the fiber's surface. The first one is dominant when approaching the center of the fiber while the second one is dominant near the fiber's free surface and decays on moving toward the fiber's center. **Figure 9** shows the difference between the paths of optical rays through the bent fiber in the compressed and expanded parts. The stress release was supposed to have a radial dependence on the fiber's radius, which enabled the construction of 2D RIP of the investigated bent homogeneous optical fiber. Based on the expected stress values due to the bending effect, a function describing the RIP was proposed and used to integrate the optical path of the ray traversing the fiber [50]. By adapting the appropriate parameters of this function, the optical phase differences were estimated and matched those phase differences that were experimentally obtained. By this assumption, a realistic induced stress profile due to bending was obtained [33]. DHPSI was used in that study where the recorded phase shifted holograms were combined and processed to extract the phase map of the fiber [18]. By considering both of the mentioned effects, the following function was chosen to describe the RIP of the bent optical fiber [33].

$$n(x,r) = -\rho n_{bf}\frac{x}{R}\left[1 - e^{-\left(\frac{r_Q - r}{r_s}\right)}\right] + n_{cl} \tag{18}$$

where ρ is the strain-optic coefficient, n_{bf} is the refractive index of the bent-free fiber, R is the radius of bending, r_o is the radius of the fiber, n_{cl} is the clad's refractive index, r_s is the proposed parameter to control the distance suffering stress release from the surface of the fiber, and x is the distance between the center of the fiber and the position of the incident ray.

The first term of Eq. (18) gives the bent-induced birefringence,

$$\Delta n(x,r) = -\rho n_{bf}\frac{x}{R}\left[1 - e^{-\left(\frac{r_Q - r}{r_s}\right)}\right] \tag{19}$$

which is correlated to the generated stress $S\ (r,x)$ inside the fiber

$$S(r,x) = E\left(\frac{-\Delta n(x,r)}{\rho n_{bf}}\right) = E\frac{x}{R}\left[1 - e^{-\left(\frac{r_Q - r}{r_s}\right)}\right] \tag{20}$$

Eq. (20) evaluates the distribution of stress over the fiber's cross-section for different bending radii where E is the Young's modulus of the bent fiber. The signs of Δn are opposite to the signs of tensile and compressive stresses. The tensile stress was chosen to be positive.

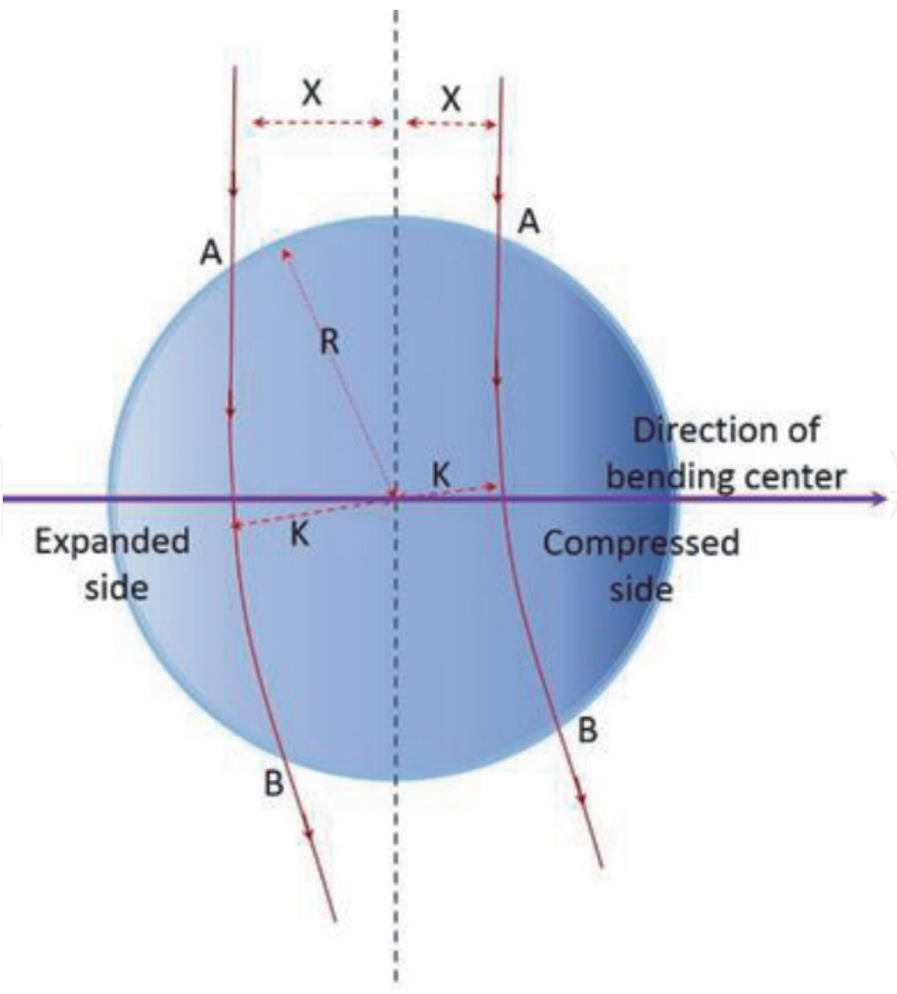


Figure 9.
A schematic diagram shows the path of an optical ray crossing a bent homogeneous optical fiber.

Since bending such a step-index optical fiber converts it into a weekly graded-index fiber, Bouguer's formula [40] was used to correlate the radius, incidence angles, and refractive index of the bent fiber as follows:

$$Kn(x,K) = rn(x,r)\sin\theta_r \tag{21}$$

where $n(x,r)$ is the refractive index at radius r. By applying this formula at the incidence point, one obtains

$$Kn(x,K) = r_o n_L \frac{x}{r_o} = xn_L \tag{22}$$

This equation was numerically solved to get K satisfying the lower integration limit of the optical path difference for a certain value of x. Based on the model described in Ref. [50], the infinitesimal change in the geometrical distance along the path of the optical ray with respect to the radius variation was given as:

$$\left(\frac{\partial l}{\partial r}\right)_{n(x,r)} = \frac{2n(x,r)r}{\sqrt{n^2(x,r)r^2 - n^2(x,k)k^2}} \tag{23}$$

By integration with respect to r, the total path length inside the fiber is:

$$l(x) = 2\int_K^{r_o} \frac{n(x,r)r}{\sqrt{n^2(x.r)r^2 - (n_L x)^2}}dr \tag{24}$$

The optical path length difference between this ray, passed through the fiber, and the reference ray passed through the liquid is:

$$opld(x) = 2\int_K^{r_o} \frac{(n(x,r) - n_L)\cdot n(x,r)r}{\sqrt{n^2(x.r)r^2 - (n_L x)^2}}dr \tag{25}$$

The phase difference is given as:

$$\phi(x) = \frac{2\pi}{\lambda} opld(x) \tag{26}$$

Figure 10 shows a set of five shifted holograms of a bent step-index optical fiber with a bending radius R = 8 mm when the incident light was vibrating parallel to the fiber's axis. They were recorded in order to apply the DHPSI technique and reconstruct the RIP of the bent fiber. The 2π shifted interferogram was analyzed and its reconstructed interference phase map, enhanced phase map, and interference phase distribution are shown in **Figures 11a–c**, respectively. The refractive index cross-section distribution of the bent optical fiber is shown in **Figure 12** while the strain-optic coefficients in compression and expansion were 0.208 and 0.224, respectively.

3.2 Graded-index bent conventional optical fiber

In 2017, Ramadan et al. presented a theory to recover the RIP of a bent GR-IN optical fiber inside the core region using DHPSI [35]. They assumed the two different processes controlling the shape of the RIP: (1) the linear variation due to stresses in the direction of the bent radius and (2) the release of the stresses near the fiber's surface.

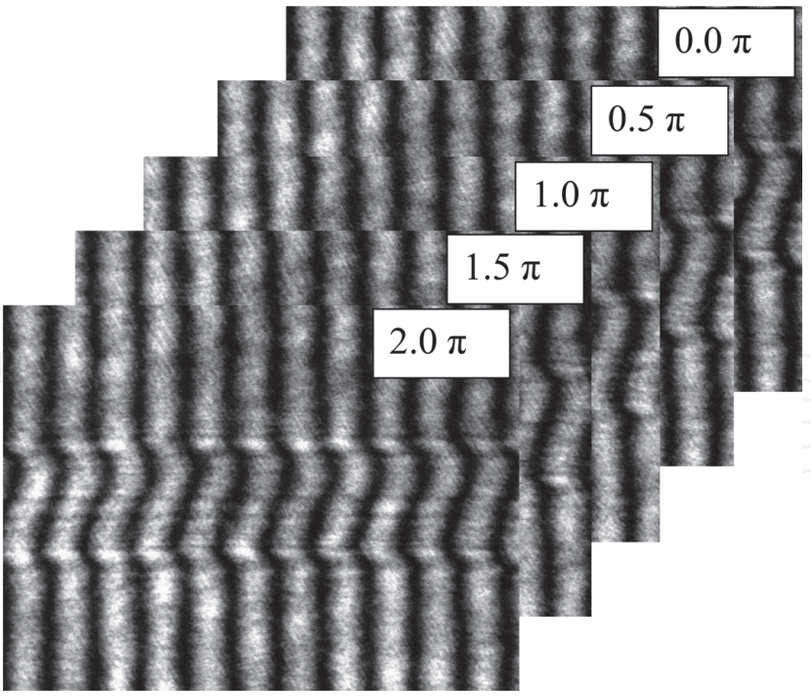


Figure 10.
A set of five shifted interferograms of a bent step-index optical fiber.

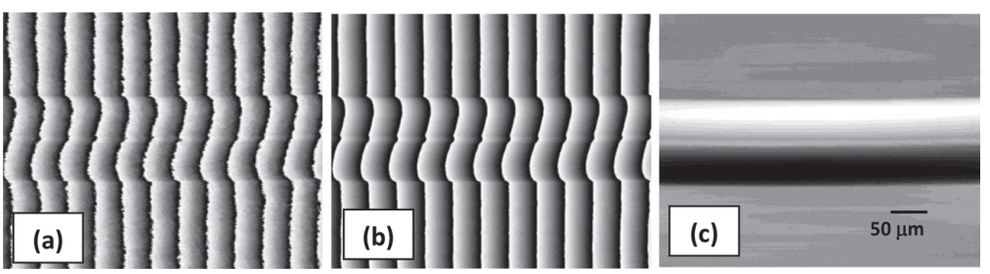


Figure 11.
(a) The reconstructed interference phase map modulo 2π, (b) its enhanced phase map, and (c) the interference phase distribution.

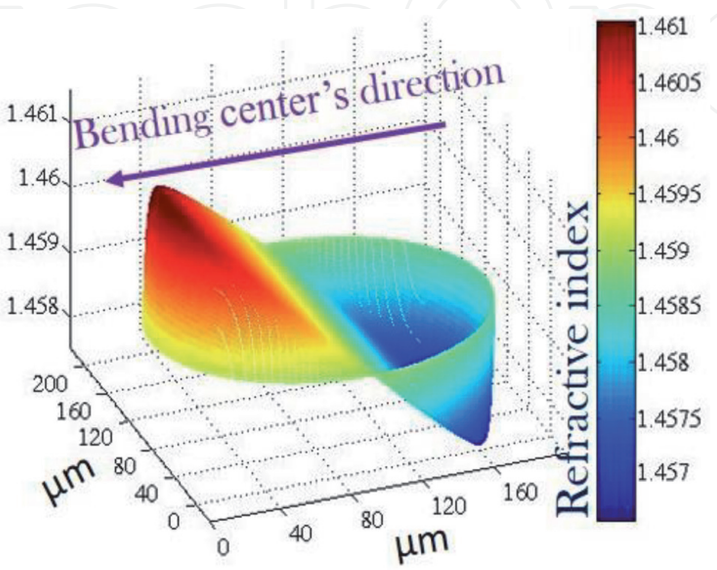


Figure 12.
The refractive index cross-section distribution of the bent optical fiber, R = *8.*

The total optical path length of the optical ray crossing the bent GR-IN optical fiber is given by Eq. (27), see **Figure 13**. The calculated optical path length differences of the interfered rays can be transformed, afterward, into a phase difference map using Eq. (26).

$$OPlD(d) = OPlD_{cl}(d) + OPlD_{c}(d) \tag{27}$$

with,

$$OPlD_{cl}(d) = 2\int_{r_c}^{r_{cl}} \frac{(n_{cl}(d,r) - n_L)n_d(d,r)r}{\sqrt{n_{cl}(d,r)^2 r^2 - n_{cl}(d,k_{cl})^2 k_{cl}^2}} dr \tag{28}$$

$$OPlD_{c}(d) = 2\int_{k_c}^{r_c} \frac{(n_{c}(d,r) - n_L)n_c(d,r)r}{\sqrt{n_{c}(d,r)^2 r^2 - n_{c}(d,k_{c})^2 k_{c}^2}} dr \tag{29}$$

Figure 14a shows a set of five phase shifted interferograms for the bent GR-IN optical fiber with bending radius R = 8 mm when the incident light was vibrating parallel to the fier's axis. The enhanced reconstructed phase modulo 2π and the interference phase distribution of the bent fiber are shown in **Figure 14b**. Due to

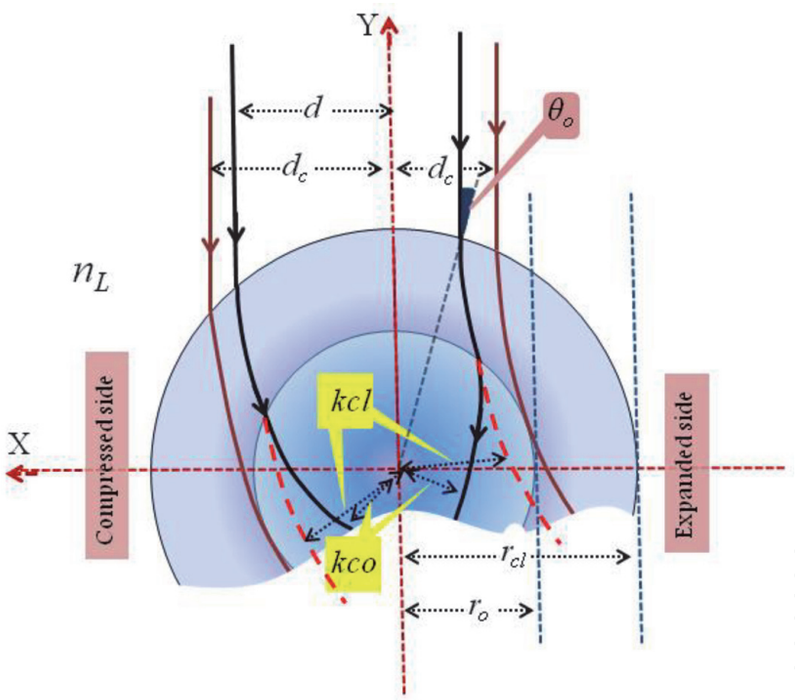


Figure 13.
schematic diagram shows the ray tracing in case of traversing bent GR-IN fiber.

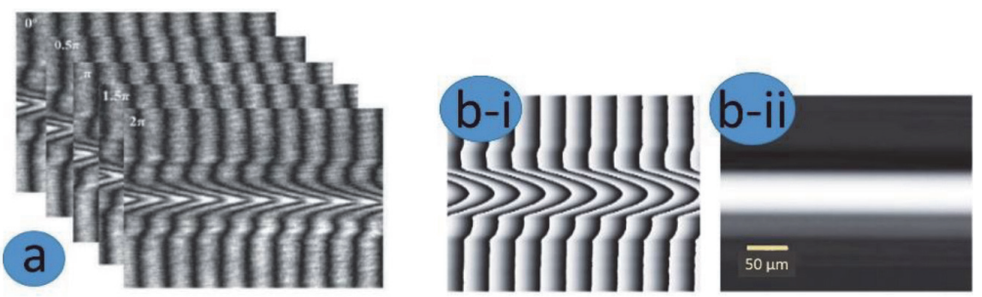


Figure 14.
(a) A set of five phase shifted interferograms of a bent GR-IN optical fiber. (b) The enhanced reconstructed phase modulo 2π and the interference phase distribution. Ref. [35] with permission.

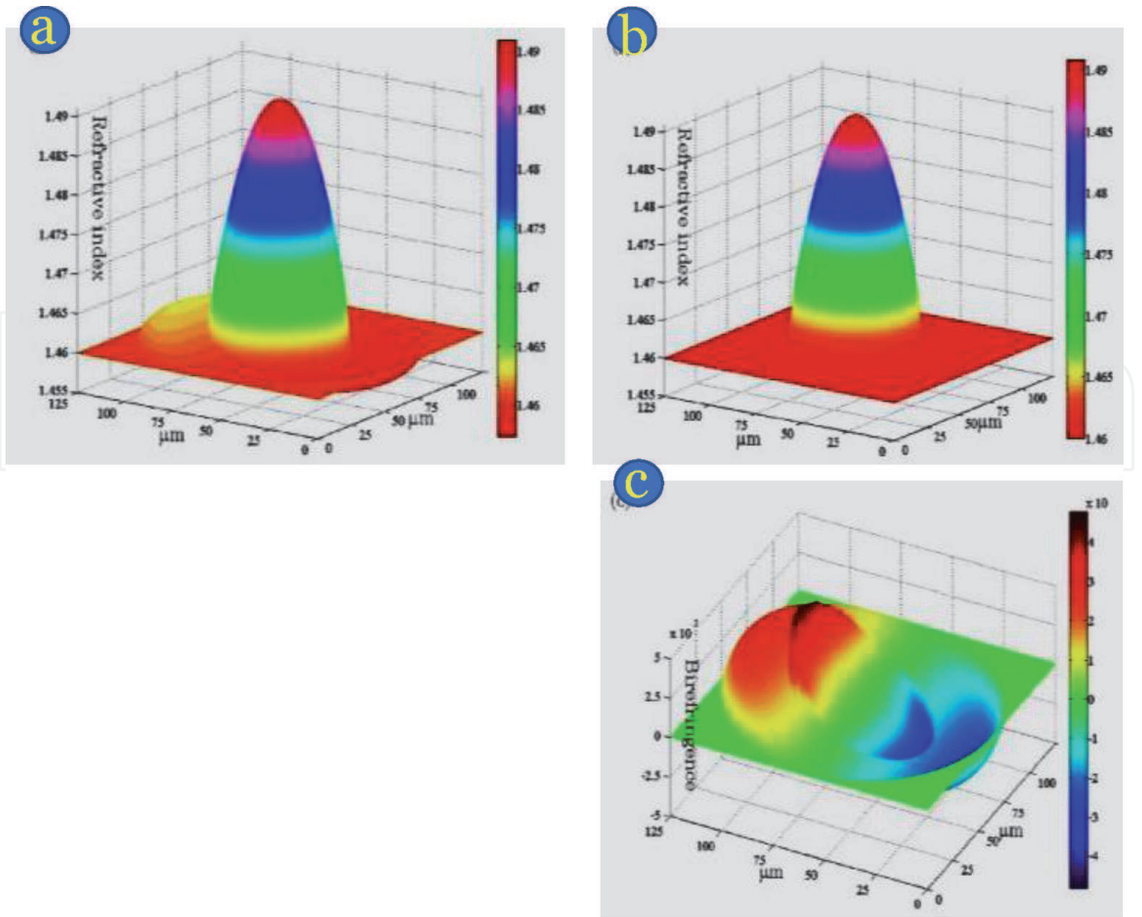


Figure 15.
Refractive index cross-section distribution of the bent GR-IN optical fiber when the incident light vibrates (a) parallel and (b) perpendicular to the fiber's axis. (c) The birefringence cross-section distribution, R = *8 mm. Ref. [35] with permission.*

the bending process, the GR-IN optical fiber exhibited a birefringence where the RIPs when the incident light vibrated parallel and perpendicular to the fiber's axis were different, see **Figure 15**.

4. Polarization maintaining (PM) optical fibers

A PM fiber is any fiber that preserves and transmits the polarization state of the light launched into the fiber even if this fiber is subjected to environmental

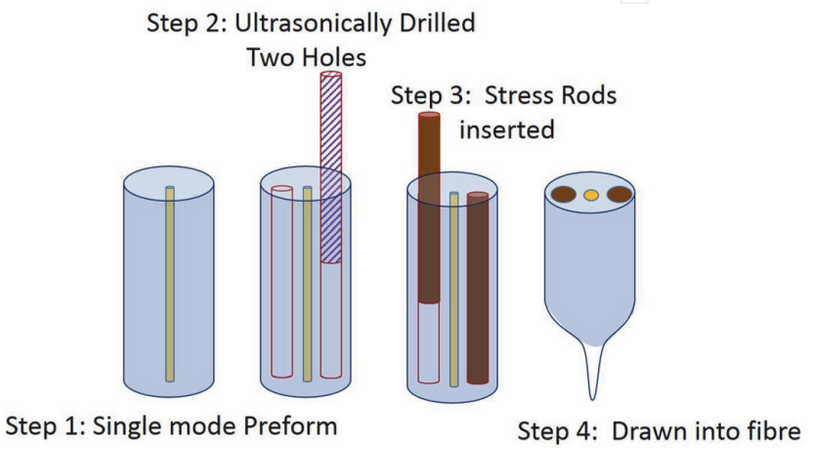


Figure 16.
Manufacturing steps of a PANDA PM optical fiber.

perturbations [57]. This advantage cannot be verified by conventional single-mode optical fibers outside the laboratory conditions. A PM fiber is tailored to oblige the two orthogonally polarized modes traveling with different velocities (i.e., different propagation constants). This difference in velocities prevents the optical energy from suffering a "cross-coupling" and preserves the polarization state of the transmitted light. Therefore, a PM fiber used in any application requires delivering a polarized light such as in telecommunications, medical applications, and sensing.

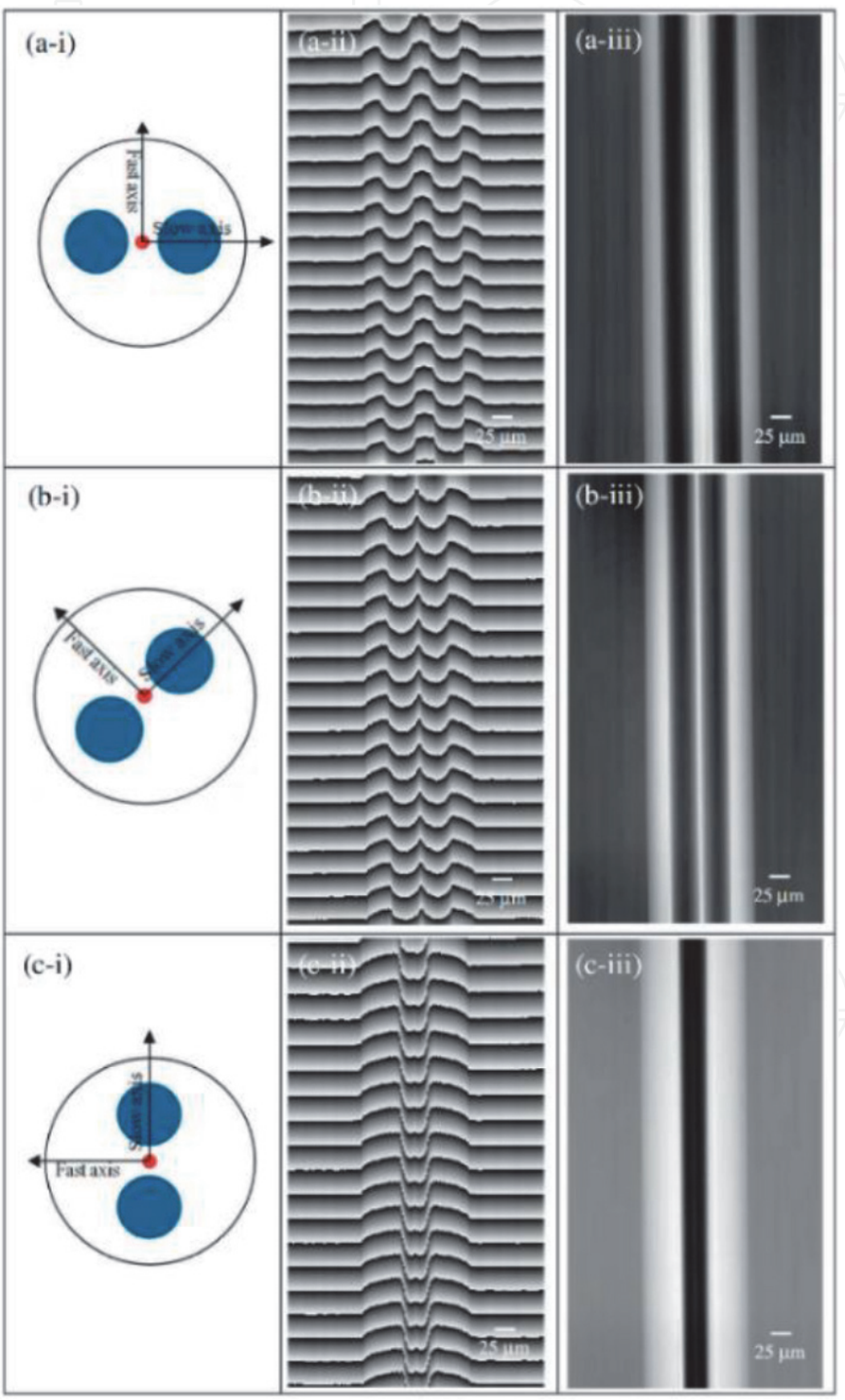


Figure 17.
The left column shows three orientations of PANDA PM optical fiber as it was rotated during the characterization process where the slow axis makes an angle (a-i) 0°, (b-i) 45° and (c-i) 90° with the horizontal axis. The middle column shows their reconstructed interference phase modulo 2π while the right column shows their phase difference maps. Ref. [23] with permission.

In interferometric applications, it is used to affirm that the interfered rays have the same polarization states. To maintain such a difference of velocities, the core of the fiber has to be anisotropic either geometrically by making the core cross-section as an ellipse or by applying a uniaxial stress. The most known PM fibers used today are, PANDA, bow tie, and elliptical-jacket fibers. These types are designed by the same way where the cores are flanked by areas of high-expansion glass and shrunk-back more than the surrounding silica then the core is frozen under tension. The birefringence is induced due to this tension, which means creation of two different indices of refraction: a higher index in the direction parallel to the applied stress and a lower index perpendicular to the direction of the applied stress. In the next two subsections, we briefly illustrate both the manufacturing process and interferometric characterization of PANDA and bow tie PM optical fibers.

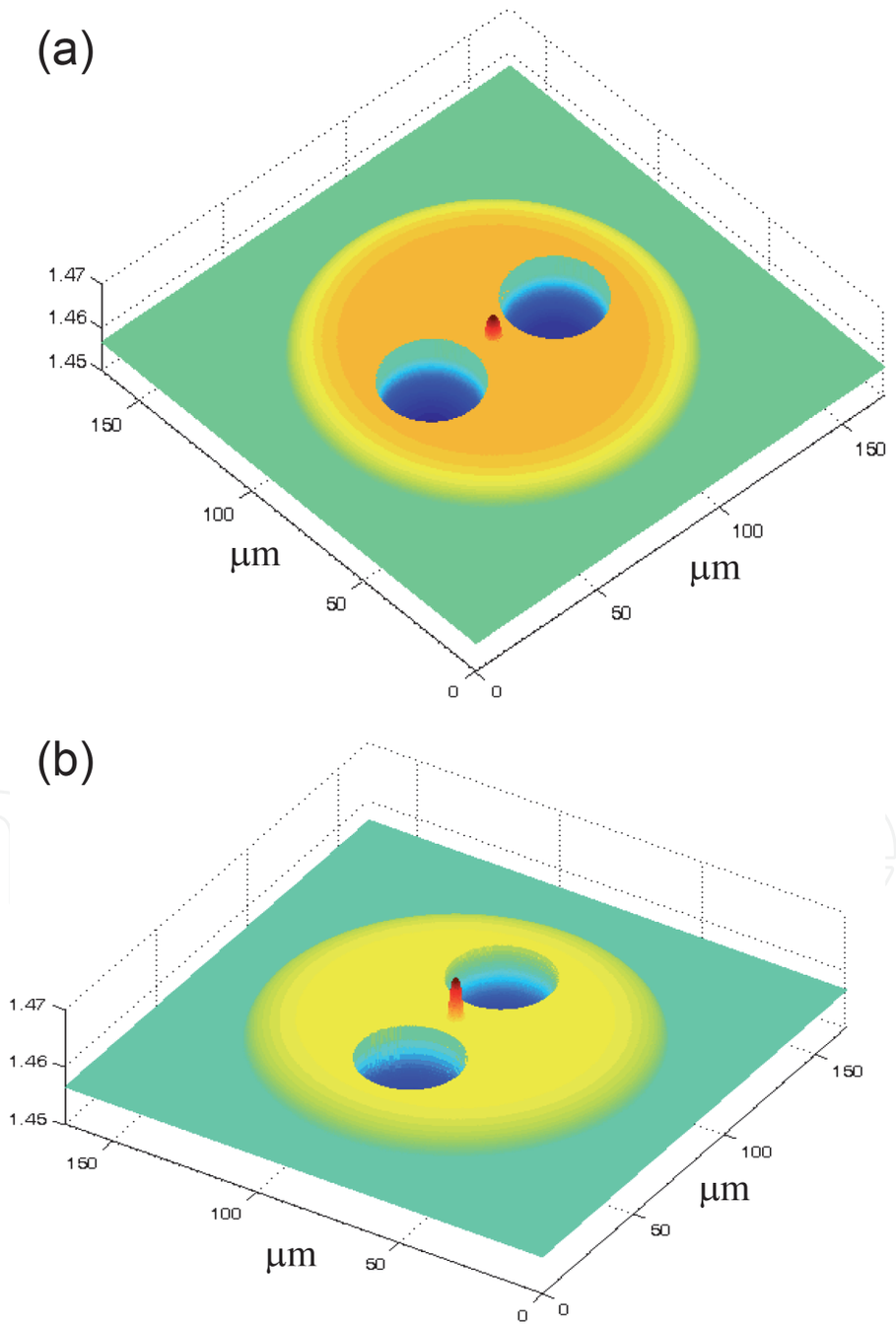


Figure 18.
The 3D RIPs of PANDA PM optical fiber in the directions of (a) fast axis and (b) slow axes. Ref. [23] with permission.

4.1 Panda optical fiber

PANDA PM optical fiber is preferable in telecommunications [57, 58]. It is modified by insertion of stress rods to provide PM properties according to the procedure described in **Figure 16**. In this process, two holes are ultrasonically

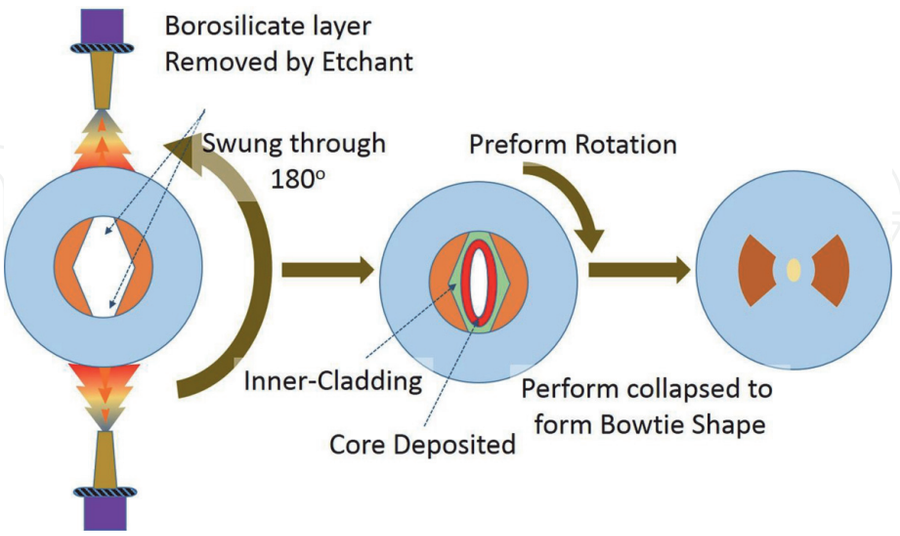


Figure 19.
Manufacturing steps of a bow tie PM optical fiber.

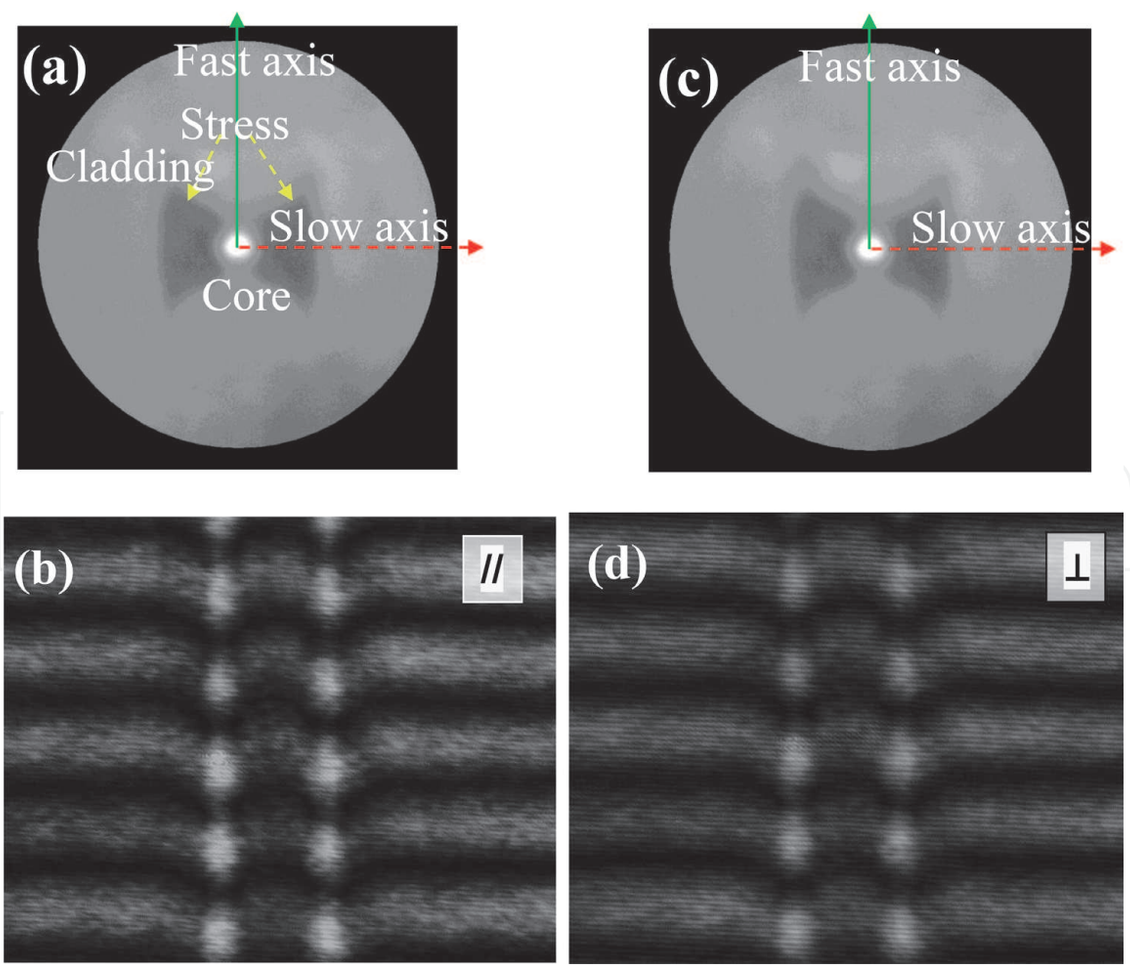


Figure 20.
(a and c) Cross-sections of the bow tie optical fiber. (b and d) Experimentally obtained phase shifted interferograms when the incident light vibrates parallel and perpendicular to fiber's axis, respectively. Ref. [59] with permission.

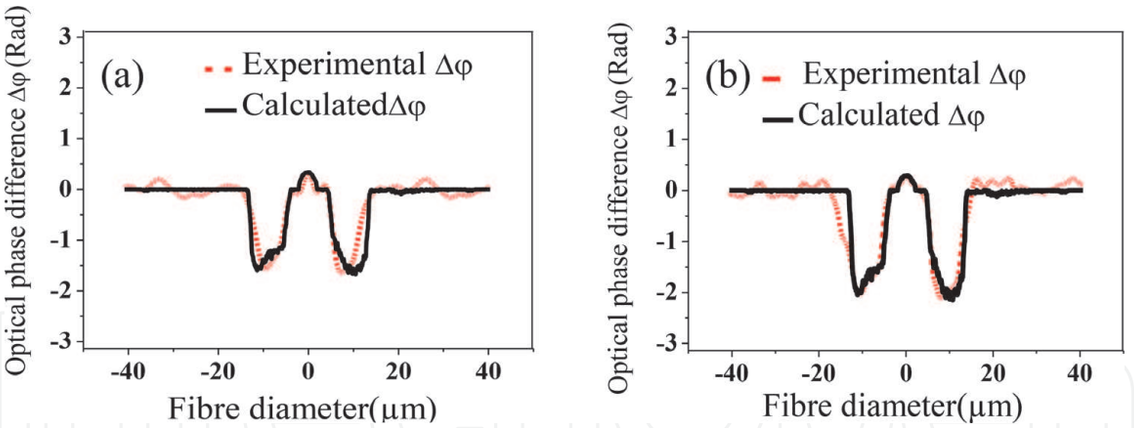


Figure 21.
The calculated and the experimental phase differences of the bow tie optical fiber when the incident light vibrates (a) parallel and (b) perpendicular to the fiber's axis. Ref. [59] with permission.

drilled along a single-mode optical fiber; then, the stress rods are inserted in these two holes and the fiber is finally drawn [57]. In 2014, Wahba used the off-axis DHPSI to reconstruct the 3D RIP of a PM PANDA optical fiber [23]. The multilayer model was used to calculate the RIP of this fiber in the directions of fast and slow axes. By rotating the PANDA fiber, different interferograms were recorded and analyzed in order to reconstrut the 3D RIP of this fiber, see **Figure 17**. The reconstructed 3D RIPs of PANDA fiber are shown in **Figure 18** when the incident light was vibrating in the direction of (a) fast axis and (b) slow axis.

4.2 Bow tie optical fiber

A bow tie optical fiber is fabricated on a lathe using the inside vapor-phase oxidation (IVPO) via the process called gas-phase etching to create the required stress [57]. This process is summarized in **Figure 19** where a ring of boron-doped silica is purely deposited of boron tribromide in combination with silicon tetrachloride. The rotation of the lathe stopped when a sufficiently thick layer was formed to allow two diametrically opposed sections to be etched away. The final shape of the bow tie and stress levels are controlled by varying the arc through which the etching burner is rotated. Recently, Ramadan et al. estimated the optical phase variations of optical rays traversing a PM optical fiber from its cross-section images [59]. They proposed an algorithm to recognize the different areas of the fiber's cross-section, which was immersed in a matching liquid and investigated by Mach-Zehnder interferometer.

These areas were scanned to calculate the optical paths for certain values of refractive indices and the optical phases across the PM optical fiber were recovered. The experimental interferograms of the bow tie PM optical fiber, shown in **Figure 20**, were analyzed to extract their optical phase distributions and compare them with the optimized estimated optical phase maps, see **Figure 21**. This was a direct and accurate method to get information about refractive index, birefringence, and the beat length of a PM optical fiber.

5. Homogeneous thick optical fibers

Optical fibers having diameters in the order of 100 μm, or less, are convenient to be investigated using interferometric methods when the samples are put in immersion liquids of refractive indices close to the refractive indices of the fibers as

described in the previous sections [12, 13]. Optical fibers of diameters bigger than 150 μm cannot be investigated by normal interferometry where the planes of fringes in both liquid and fiber cannot be focused simultaneously. In 2000, Ramadan presented a novel interferometric method to recover such a problem for homogeneous thick optical fibers, commonly used in short-distance data transmission, without using immersion liquids [16]. This type of interference was called lens-fiber interferometry (LFI) since the interference fringes were produced by a combination of an aberrated cylindrical lens and a thick optical fiber. The aberrated cylindrical lens was used to focus a parallel beam on this fiber, which was located in the focal plane of the cylindrical lens [60], see **Figure 22**.

Two-beam interference produced by the superposition of two optical rays emerging from the fiber was recorded and explained. Due to the aberration of the cylindrical lens, one of these two rays crossed the thick fiber before its center while the other ray crossed after the fiber's center. Therefore, for each point in the image plane, two rays having two different initial incidence angles on the thick fiber are superposed, see **Figure 23**. The optical path length of each ray can be obtained by tracing this ray geometrically, as given by Eq. (30), which can be transformed into phase differences for the interfered rays using Eq. (31). The difference in the optical path lengths of each pair of interfered rays can be transformed into an intensity distribution describing the interference fringes using Eq. (32). On the other hand, the scattered rays from the outer surface of the fiber do not contribute in the interference because of the limited range of the incident rays on the fiber. This is in contrast with previous works done by Watkins [14, 15, 61]. By comparing the experimentally obtained interferograms with those reconstructed theoretically as

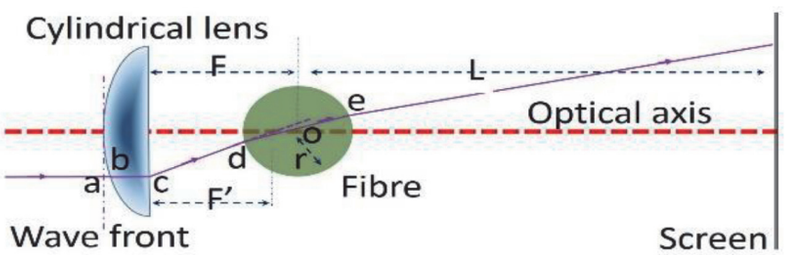


Figure 22.
The ray tracing diagram of an optical ray crossing a homogeneous thick optical fiber.

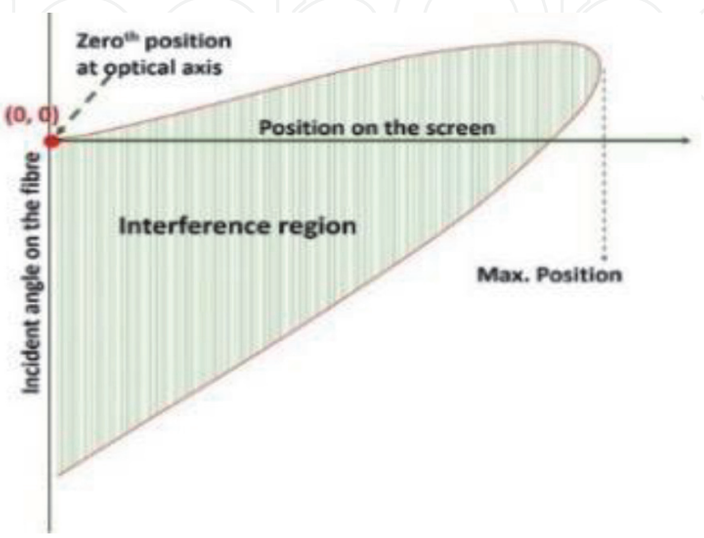


Figure 23.
The relation between the position of each two interfered rays on the screen and their incidence angles on the thick fiber.

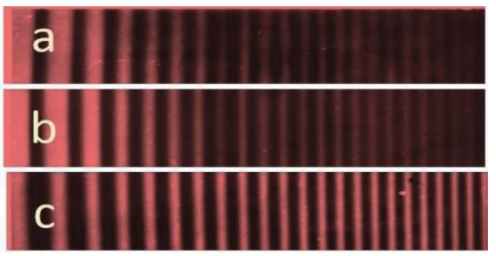


Figure 24.
(a) A selected and extended part of the obtained interferogram of a thick optical fiber, (b) the enhanced fringes of (a) and (c) the simulated fringes.

shown in **Figure 24**, Ramadan was able to determine the refractive index of the investigated thick optical fiber. The advantage is that the used system requires no matching liquid where the experiment is performed when the thick fiber is just held in air. This enables monitoring the probable variation in radius or refractive index of the fiber particularly during the manufacturing process or under external effects.

$$\Delta(z) = ab + bc \cdot n_L + cd + de \cdot n_f + ep \tag{30}$$

$$\delta = \frac{2\pi}{\lambda} \cdot (\Delta(z_1) - \Delta(z_2)) \tag{31}$$

$$I = 4A^2 \cos^2\left(\frac{\delta}{2}\right) \tag{32}$$

where $\Delta(z_1)$ and $\Delta(z_2)$ are the optical path lengths of the two interfered rays. In 2004, Hamza et al. developed LFI technique in order to determine the refractive index of the core of a skin-core thick optical fiber [60]. They derived a mathematical expression for the optical paths through the fiber in order to reconstruct the interfernce pattern due to the used fiber when it is used as a thick fiber in the LFI system. By comparing the experimentally obtained patterns with the theoretically reconstructed ones, they were able to estimate the core's refractive index with an accuracy of 8×10^{-4}. Due to its simplicity and applicability, LFI was used, afterward, to measure the refractive index of a liquid [62] and to monitor the thickness variations of a transparent sheet inserted between the cylindrical lens and the thick fiber [63].

6. Conclusions

This chapter is an attempt to highlight the interferometric techniques used for characterization of optical fibers. Application of two- and multiple-beam interference on different types of fibers is illustrated. Section 2 dealt with conventional optical fibers where we illustrated the theoretical models used to reconstruct the refractive index profiles of these fibers. In these models, the refraction of the light ray traversing the fiber has been considered. Digital holography was explained as an important candidate used for accurate retrieving of phase maps and consequently refractive index profiles of the fibers. In Section 3, we mentioned the problem of fiber bending. Recovering the refractive index profile and mode propagation of a bent fiber considering the refraction of the light rays traversing the fiber is a quite difficult task since bending-induced stresses are responsible for refractive index variations. Also, these stresses are released at the outer surface of the bent fiber. Therefore, we illustrated a successful model that was recently presented to recover the index profile in this case with experimental illustrative data. Another important

type of optical fibers is the polarization maintaining optical fibers, which prevent cross-coupling by conserving the state of beam polarization during propagation. In Section 4, we presented interferometric techniques applied on two different polarization maintaining optical fibers, panda and bow tie, to reconstruct their refractive index profiles. Most interference techniques require immersing the fiber in a suitable liquid in order to minimize the phase difference between the fiber and its surrounding medium. In Section 5, an interference technique is presented and applied on a thick optical fiber to recover its refractive index without using an immersion liquid (i.e., in air), which makes the technique suitable for in-situ studying of thick fibers.

Acknowledgements

The authors would like to acknowledge Prof. A. Hamza, the leader of optics research groups in Mansoura and Damietta Universities, and Prof. T. Sokkar for their continuous support and useful discussions. Also, many thanks to the Optics Research Group members in Damietta University for their useful suggestions and comments.

Conflict of interest

The authors declare no conflict of interest.

Author details

Hamdy Wahba[1,2*], Wael Ramadan[1] and Ahmed El-Tawargy[1]

1 Physics Department, Faculty of Science, Damietta University, New Damietta, Egypt

2 Physics Department, Faculty of Science, Taif University, Taif, Saudi Arabia

*Address all correspondence to: hhwahba76@gmail.com

IntechOpen

© 2020 The Author(s). Licensee IntechOpen. This chapter is distributed under the terms of the Creative Commons Attribution License (http://creativecommons.org/licenses/by/3.0), which permits unrestricted use, distribution, and reproduction in any medium, provided the original work is properly cited. CC BY

References

[1] El-Diasty F. Characterization of optical fibers by two- and multiple-beam interferometry. Optics and Lasers in Engineering. 2008;**46**:291-305. DOI: 10.1016/j.optlaseng.2007.10.004

[2] Midwinter JE. Optical Fibers for Transmission. New York: Wiley; 1979

[3] Barakat N, Hamza AA. Interferometry of Fibrous Materials. Bristol, New York: A. Hilger; 1990

[4] DeCusatis C. Optical data communication: Fundamentals and future directions. Optical Engineering. 1998;**37**:3082. DOI: 10.1117/1.601993

[5] Udd E, Spillman WB, editors. Fiber Optic Sensors: An Introduction for Engineers and Scientists. Hoboken, NJ, USA: John Wiley & Sons, Inc.; 2011. DOI: 10.1002/9781118014103

[6] Hall DR, Jackson PE, editors. The Physics and Technology of Laser Resonators. Bristol, New York: A. Hilger; 1989

[7] Erdogan T. Fiber grating spectra. Journal of Lightwave Technology. 1997; **15**:1277-1294. DOI: 10.1109/50.618322

[8] Meltz G, Morey WW, Glenn WH. Formation of Bragg gratings in optical fibers by a transverse holographic method. Optics Letters. 1989;**14**:823. DOI: 10.1364/OL.14.000823

[9] Hill KO, Malo B, Vineberg KA, Bilodeau F, Johnson DC, Skinner I. Efficient mode conversion in telecommunication fibre using externally written gratings. Electronics Letters. 1990;**26**:1270. DOI: 10.1049/el: 19900818

[10] De Paula RP, Moore EL. In: Moore EL, Ramer OG, editors. Review of All-Fiber Phase and Polarization Modulators. Arlington, United States: SPIE. Digital library, Technical Symposium East; 1984. p. 3. DOI: 10.1117/12.942649

[11] El-Sherif MA. On-fiber sensor and modulator. IEEE Transactions on Instrumentation and Measurement. 1989;**38**:595-598. DOI: 10.1109/ 19.192356

[12] Hamza AA, Ghander AM, Sokkar TZN, Mabrouk MA, Ramadan WA. On the determination of the refractive index of a fibre: I. Skin-core fibre. Pure and Applied Optics. 1994;**3**:943-961. DOI: 10.1088/ 0963-9659/3/6/003

[13] Hamza AA, Sokkar TZN, Ghander AM, Mabrouk MA, Ramadan WA. On the determination of the refractive index of a fibre. II. Graded index fibre. Pure and Applied Optics. 1995;**4**:161-177. DOI: 10.1088/ 0963-9659/4/3/004

[14] Watkins LS. Scattering from side-illuminated clad glass fibers for determination of fiber parameters. Journal of the Optical Society of America. 1974;**64**:767. DOI: 10.1364/ JOSA.64.000767

[15] Watkins LS. Laser beam refraction traversely through a graded-index preform to determine refractive index ratio and gradient profile. Applied Optics. 1979;**18**:2214. DOI: 10.1364/ AO.18.002214

[16] Ramadan WA. On-line lens-fibre interference method for testing a thick fibre. Journal of Optics A: Pure and Applied Optics. 2000;**2**: 234-238. DOI: 10.1088/1464-4258/2/ 3/311

[17] Wahba HH, Kreis T. In: Lehmann PH, editor. Characterization

of Optical Fibers by Digital Holographic Interferometry. Munich, Germany: SPIE. Digital library, Europe Optical Metrology; 2009. p. 73890K. DOI: 10.1117/12.826854

[18] Wahba HH, Kreis T. Digital holographic interferometric characterization of bent optical fibers. Journal of Optics A: Pure and Applied Optics. 2009;**11**:105407. DOI: 10.1088/1464-4258/11/10/105407

[19] Wahba H. Digital Holography and Interferometric Metrology of Optical Fibres Digital Holographic Phase Shifting and Interferometric Characterization of Optical Fibers. VDM Verlag Dr. Müller: Saarbrücken; 2011

[20] El-Din MAS, Wahba HH. Investigation of refractive index profile and mode field distribution of optical fibers using digital holographic phase shifting interferometric method. Optics Communications. 2011;**284**:3846-3854. DOI: 10.1016/j.optcom.2011.04.037

[21] Wahba H, Shams M. Digital holographic interferometric characterization of optical waveguides. In: Naydenova I, editor. Advanced Holography - Metrology and Imaging. InTech; 2011. DOI: 10.5772/22311

[22] Sokkar TZN, Ramadan WA, Shams El-Din MA, Wahba HH, Aboleneen SS. Bent induced refractive index profile variation and mode field distribution of step-index multimode optical fiber. Optics and Lasers in Engineering. 2014; **53**:133-141. DOI: 10.1016/j.optlaseng.2013.09.002

[23] Wahba HH. Reconstruction of 3D refractive index profiles of PM PANDA optical fiber using digital holographic method. Optical Fiber Technology. 2014;**20**:520-526. DOI: 10.1016/j.yofte.2014.06.002

[24] Sokkar TZN, El-Farahaty KA, Ramadan WA, Wahba HH, Raslan MI, Hamza AA. Nonray-tracing determination of the 3D refractive index profile of polymeric fibres using single-frame computed tomography and digital holographic interferometric technique: Single frame computed tomography. Journal of Microscopy. 2015;**257**: 208-216. DOI: 10.1111/jmi.12203

[25] Ramadan WA, El-Tawargy AS. A double image Mach–Zehnder interferometer. Applied Physics B. 2015; **118**:203-208. DOI: 10.1007/s00340-014-5970-3

[26] Wahba HH, Kreis T. Characterization of graded index optical fibers by digital holographic interferometry. Applied Optics. 2009; **48**:1573. DOI: 10.1364/AO.48.001573

[27] Yassien KM, Agour M, von Kopylow C, El-Dessouky HM. On the digital holographic interferometry of fibrous material, I: Optical properties of polymer and optical fibers. Optics and Lasers in Engineering. 2010;**48**:555-560. DOI: 10.1016/j.optlaseng.2009.12.003

[28] Wahba HH, Shams El-Din MA. In: Lehmann PH, Osten W, Gastinger K, editors. Reconstruction of 3D refractive index distribution across the graded index optical fibre using digital holographic interferometry. Munich, Germany; 2011. p. 80822B. DOI: 10.1117/12.882164

[29] Wahba HH, Sjödahl M, Gren P, Olsson E. High resolution digital holographic microscopy for the study of aggregated natural cellulose nanowhisker fibers. Optics and Lasers in Engineering. 2015;**73**:69-74. DOI: 10.1016/j.optlaseng.2015.04.005

[30] Sokkar TZN, Shams El-Din MA, El-Tawargy AS. Effect of recycling on the optical, mechanical and structural properties of polypropylene fibers. Optics and Lasers in Engineering. 2013; **51**:994-1003. DOI: 10.1016/j.optlaseng.2013.02.018

[31] El-Morsy MA, Yatagai T, Hamza A, Mabrouk MA, Sokkar TZN. Multiple-beam Fizeau fringe-pattern analysis using Fourier transform method for accurate measurement of fiber refractive index profile of polymer fiber. Journal of Applied Polymer Science. 2002;**85**: 475-484. DOI: 10.1002/app.10387

[32] Shams El-Din MA, El-Tawargy AS. Interferometric study of the effect of laser intensity and polarization on the cold-drawing of virgin polypropylene fibres. Indian Journal of Physics. 2017; **91**:1425-1435. DOI: 10.1007/s12648-017-1044-9

[33] Ramadan WA, Wahba HH, Shams El-Din MA. Two-dimensional refractive index and stresses profiles of a homogenous bent optical fiber. Applied Optics. 2014;**53**:7462. DOI: 10.1364/AO.53.007462

[34] Sokkar TZN, Shams El-Din MA, El-Tawargy AS. On Young's modulus profile across anisotropic nonhomogeneous polymeric fibre using automatic transverse interferometric method. Optics and Lasers in Engineering. 2012;**50**:1223-1229. DOI: 10.1016/j.optlaseng.2012.03.017

[35] Ramadan WA, Wahba HH, Shams El-Din MA. Two-dimensional refractive index and birefringence profiles of a graded index bent optical fibre. Optical Fiber Technology. 2017;**36**:115-124. DOI: 10.1016/j.yofte.2017.03.005

[36] Hamza AA, Mabrouk MA. A multiple-beam interferometric method for refractive index determination of graded optical fibres. Journal of Modern Optics. 1991;**38**:97-107. DOI: 10.1080/09500349114550131

[37] Hamza AA, Sokkar TZN, El-Morsy MA, Nawareg MAE. Automatic determination of refractive index profile of fibers having regular and/or irregular transverse sections considering the refraction of light rays by the fiber. Optics Communications. 2009;**282**: 27-35. DOI: 10.1016/j.optcom.2008.09.073

[38] Hamza AA, Sokkar TZN, El-Morsy MA, Nawareg MAE. Automatic determination of refractive index profile, sectional area, and shape of fibers having regular and/or irregular transverse sections. Optics & Laser Technology. 2008;**40**:1082-1090. DOI: 10.1016/j.optlastec.2008.01.022

[39] Ramadan WA. Intensity distribution of Fizeau fringes in transmission with the real path of the interfered multiple-beams. Optics and Lasers in Engineering. 2014;**58**:27-32. DOI: 10.1016/j.optlaseng.2014.01.017

[40] Born M, Wolf E. Principles of Optics: Electromagnetic Theory of Propagation, Interference and Diffraction of Light. 7th Expanded Ed. Cambridge. New York: Cambridge University Press; 1999

[41] Gabor D. A new microscopic principle. Nature. 1948;**161**:777-778. DOI: 10.1038/161777a0

[42] Microscopy by reconstructed wave-fronts. Proceedings of the Royal Society of London A. 1949;**197**:454-487. DOI: 10.1098/rspa.1949.0075

[43] Gabor D. Microscopy by reconstructed wave fronts: II. Proceedings of the Physical Society. Section B. 1951;**64**:449-469. DOI: 10.1088/0370-1301/64/6/301

[44] Powell RL, Stetson KA. Interferometric vibration analysis by Wavefront reconstruction. Journal of the Optical Society of America. 1965;**55**: 1593. DOI: 10.1364/JOSA.55.001593

[45] Kreis T. Holographic Interferometry: Principles and Methods. Berlin: Akademie Verlag; 1996

[46] Schnars U. Direct phase determination in hologram

interferometry with use of digitally recorded holograms. Journal of the Optical Society of America. A. 1994;**11**:2011. DOI: 10.1364/JOSAA.11.002011

[47] Schnars U. Digital recording and numerical reconstruction of holograms: Reduction of the spatial frequency spectrum. Optical Engineering. 1996;**35**:977. DOI: 10.1117/1.600706

[48] Schnars U, Jueptner W. Digital Holography: Digital Hologram Recording, Numerical Reconstruction, and Related Techniques. Berlin: Springer; 2005

[49] Hariharan P, Oreb BF, Brown N. Real-time holographic interferometry: A microcomputer system for the measurement of vector displacements. Applied Optics. 1983;**22**:876. DOI: 10.1364/AO.22.000876

[50] Hamza AA, Mabrouk MA, Ramadan WA, Shams-Eldin MA. Determination of GR-IN optical fibre parameters from transverse interferograms considering the refraction of the incident ray by the fibre. Optics Communications. 2001;**200**:131-138. DOI: 10.1016/S0030-4018(01)01561-9

[51] Mabrouk MA. Two-beam interference detection of the changes in fibre structural parameters during low drawing process. Polymer Testing. 2002;**21**:897-904. DOI: 10.1016/S0142-9418(02)00026-0

[52] Fan Y, Wu G, Wei W, Yuan Y, Lin F, Wu X. Fiber-optic bend sensor using LP_21 mode operation. Optics Express. 2012;**20**:26127. DOI: 10.1364/OE.20.026127

[53] Méndez A, Morse TF. Specialty Optical Fibers Handbook. Amsterdam [u.a.]: Elsevier/Academic Press; 2007

[54] Yin S, Ruffin PB, Yu FTS. Fiber Optic Sensors. S.l.: CRC Press; 2019

[55] Vogler DE, Lorencak A, Rey JM, Sigrist MW. Bending loss measurement using a fiber cavity ringdown scheme. Optics and Lasers in Engineering. 2005;**43**:527-535. DOI: 10.1016/j.optlaseng.2004.03.012

[56] Makouei S, Oskouei MS, Rostami A. Study of bending loss and mode field diameter in depressed inner core triple-clad single-mode optical fibers. Optics Communications. 2007;**280**:58-67. DOI: 10.1016/j.optcom.2007.07.052

[57] Emslie C. Polarization maintaining fibers. In: Specialty Optical Fibers Handbook. Elsevier; 2007. pp. 243-277. DOI: 10.1016/B978-012369406-5/50010-2

[58] Hosaka T, Okamoto K, Miya T, Sasaki Y, Edahiro T. Low-loss single polarisation fibres with asymmetrical strain birefringence. Electronics Letters. 1981;**17**:530. DOI: 10.1049/el:19810371

[59] Ramadan WA, Wahba HH, Shams El-Din MA, Abd El-Sadek IG. Refractive index retrieving of polarization maintaining optical fibers. Optical Fiber Technology. 2018;**40**:69-75. DOI: 10.1016/j.yofte.2017.11.007

[60] Hamza AA, Mabrouk MA, Ramadan WA, Wahba HH. Core-index determination of a thick fibre using lens-fibre interference (LFI) technique. Optics and Lasers in Engineering. 2004;**42**:121-130. DOI: 10.1016/j.optlaseng.2003.09.002

[61] Watkins LS. Effect of noncircular cross section on the forwardscattering pattern of side-illuminated unclad fibers. Applied Optics. 1979;**18**:4089. DOI: 10.1364/AO.18.004089

[62] Ramadan WA, Wahba HH. Lens–fibre interference in measuring liquids' refractive indices. Measurement Science and Technology. 2006;**17**:215-220. DOI: 10.1088/0957-0233/17/1/033

[63] Ramadan WA, Shams El-Din MA, Wahba HH, El-Tawargy AS, Hamza AA. Lens–fibre interference proposed to monitor a transparent sheet's thickness variations. Applied Physics B: Lasers and Optics. 2014;**117**:1073-1080. DOI: 10.1007/s00340-014-5928-5

IntechOpen

IntechOpen